communications biology

A Nature Portfolio journal

Article

https://doi.org/10.1038/s42003-025-08214-5

UBE2V1 governs aging induced protein aggregation and developmental defects in oocytes and embryos

Ling Li[1,3], Ying Liu[1,3], Xi He[1], Junqing Chen[1], Xiaowei Guan[1] ✉ & Longsen Han[2] ✉

While protein aggregation is a well-documented factor in various age-related diseases, its specific impact on oocyte aging and the molecular mechanisms responsible remain poorly understood. In a mouse model of advanced maternal age, we observe that aging promotes ubiquitinated protein aggregation in oocytes and embryos. Starting with this clue, we identify that the expression of ubiquitin-conjugating enzyme (E2) UBE2V1 in oocyte increases with age and correlates with aggresome formation. We further provide evidence that UBE2V1 positively regulates protein aggregates formation in oocyte under both physiological and stress conditions. Moreover, enhanced UBE2V1 expression mimics the phenotypes observed in aged oocytes. Notably, restoring UBE2V1 expression in aged oocytes and embryos not only alleviates aggresome formation but also partly ameliorates the age-related defects in oocyte maturation and embryo development. Thus, our findings provide a mechanistic link between UBE2V1 expression, protein aggregation and developmental defects in aged oocytes and embryos.

Due to the advancement of modern societies, maternal age at the time of childbearing has dramatically increased in many countries[1]. Age is widely regarded as one of the most critical factors affecting female reproductive health, as increasing lines of evidence suggest that advanced maternal age is linked to increased risks of infertility, pregnancy loss, and stillbirth[2,3]. It is well established that the age-associated decline in female fertility is largely ascribable to a decrease in oocyte quality[4]. However, the molecular mechanisms involved and their impact on oocyte competence remain largely unknown.

A prime contributor of decreased oocyte quality with age is aneuploidy, which stems from chromosomal and spindle abnormalities during meiosis[5]. Mechanistically, factors such as progressive loss of cohesion[6,7], compromised spindle assembly checkpoints (SAC) that control chromosome alignment[8,9], and defects in microtubule dynamics[10] have been implicated in these meiotic defects. Moreover, accumulating abnormalities in the ooplasm—including altered metabolism, organelle dysfunction, and aberrant gene and protein regulation—progressively undermine oocyte quality as well[4]. In most mammals, oocytes are formed during fetal development and survive months or decades before being utilized for reproduction. During this prolonged period, oocytes increase in size during their growth phase and accumulate maternal mRNAs and proteins for the new embryos[11]. Therefore, to sustain its developmental potential, the mature oocyte must ensure the transmission of damage-free cytoplasm to the embryo.

Protein homeostasis, also known as proteostasis, involves multiple processes that coordinate protein synthesis, folding, disaggregation, and degradation. This intricate balance is essential for maintaining cellular function and overall organismal viability[12]. Protein degradation is essential for maintaining a healthy cytoplasm by removing misfolded and damaged proteins that could otherwise accumulate and disrupt cellular processes. This degradation occurs through two tightly regulated pathways, the ubiquitin-proteasome system (UPS) and autophagy-lysosome system, which are central for protein quality control[13]. Oocyte are long-lived, non-dividing cells that are particularly sensitive to the accumulation of damaged proteins. A recent study demonstrated that mouse oocytes maintain proteostasis by sequestering ubiquitinated protein aggregates within specialized compartments known as endolysosomal vesicular assemblies (ELVAs), and degrading them through the UPS and autophagy-lysosomal pathway upon oocyte maturation[14]. However, the factors regulating the formation of ELVAs and their roles in oocyte aging remain to be elucidated.

Ubiquitination is a tightly regulated process mediated by a three-step enzymatic cascade involving E1 (ubiquitin-activating enzyme), E2 (ubiquitin-conjugating enzyme), and E3 (ubiquitin ligase). Among these, E2 enzymes play a central role by facilitating the attachment of ubiquitin (Ub)

[1]Department of Human Anatomy and Histoembryology, Nanjing University of Chinese Medicine, Nanjing, China. [2]State Key Laboratory of Reproductive Medicine and Offspring Health, Nanjing Medical University, Nanjing, China. [3]These authors contributed equally: Ling Li, Ying Liu. ✉e-mail: guanxw918@njucm.edu.cn; hls@njmu.edu.cn

to target proteins[15]. Accumulating evidence indicates that several E2 enzymes exhibited dysregulated expression in aged oocytes[16]. Importantly, UBE2V1 has been reported to positively regulate protein aggregation through enhancing K63-linked ubiquitination. Unlike the canonical signaling role of K48-linked polyubiquitination in targeting substrates for proteasomal degradation, K63-linked ubiquitin chain serve as a scaffold for protein interaction and aggregation[12]. However, whether UBE2V1 modulates protein aggregation in oocytes, particularly during aging, remains unknown.

Using a model of advanced maternal age (10–12 months) in mice, we found that maternal ageing promotes protein aggregation in mouse oocytes. Through gene screening and functional analysis, we identified UBE2V1 as being upregulated at both the mRNA and protein levels during oocyte aging, potentially facilitating protein aggregation through the catalysis of K63-linked ubiquitination. Furthermore, elevated UBE2V1 expression leads to developmental defects in young oocytes and embryos, whereas restoring UBE2V1 expression mitigates the developmental defects observed in aged oocytes and embryos.

Results

Advanced maternal age favors ELVAs formation in mouse oocyte

Oocytes enter meiosis during embryogenesis and remain arrested in meiotic prophase I for extended periods, ranging from months to even decades, rendering them highly susceptible to the accumulation of protein aggregates. Recently, Zaffagnini et al demonstrated that mouse oocytes sequester detrimental proteins in specialized compartments that defined as endolysosomal vesicular assemblies (ELVAs), which are subsequently degraded upon oocyte maturation to safeguard protein homeostasis[14]. To assess the effect of maternal aging on protein aggregation in oocytes, we isolated germinal vesicle (GV) stage oocytes, as well as early embryos from young (7–8 weeks) and old (10–12 m) mice and probed them with Proteostat, a validated dye for detecting protein aggregation in oocytes[14]. Maximum intensity projection images were obtained via z-stack confocal microscopy to examine aggregate distribution[17]. In line with previous report[14], Proteostat signals were frequently observed in young GV oocyte, and gradually decreased during early embryo development (Fig. 1A, B). Strikingly, old GV oocytes displayed a substantial increase in Proteostat signals compared to their young counterparts (Fig. 1A, B). Moreover, 2-cell embryos from aged mice, which typically showed minimal Proteostat signals in the young group, exhibit persistent enrichment of Proteostat signials (Fig. 1A, B), indicating that the formation of ELVAs escalates with age in oocytes and 2-cell embryos.

Next, we explored whether protein aggregates in aged oocytes were also marked by accumulation of ubiquitinated proteins. Immunostaining with FK2, an antibody that recognizes both mono- and polyubiquitinated proteins, was performed to determine co-localization with Proteostat-positive compartments. The results (Fig. 1C) and quantification (Fig. 1D) revealed that the vast majority of Proteostat signals in aged oocytes were co-labeled by FK2, aligning with pattern observed in young oocytes. These findings demonstrate that maternal aging favors ELVAs formation in aged oocytes and embryos.

Age-dependent upregulation of UBE2V1 in oocytes

Given that ubiquitinated protein aggregates accumulate in old oocytes, we hypothesized that the ubiquitination pathway might be compromised. To investigate this further, we conducted a comparative analysis of the expression levels of 25 E2 family members between young and old oocytes. Our quantitative real-time PCR analysis identified 4 differentially expressed E2 genes: three upregulated (*Ube2c, Ube2e2, Ube2v1*) and one downregulated (*Ube2d2*) (Supplementary Fig. 1). Among these, UBE2V1 was of particular interest due to its known role in promoting protein aggregation[12].

Until now, the role of UBE2V1 during mouse oocyte meiosis had not been explored. To investigate its potential function, we first examined UBE2V1 protein accumulation and subcellular localization during meiotic maturation. Western bolt analysis of GV, MI, and MII stage oocytes, as well as 2-cell embryos, revealed significant UBE2V1 protein accumulation in GV oocytes. However, upon meiotic resumption, UBE2V1 levels sharply declined and remained consistently low post-fertilization (Supplementary Fig. 2A). Fluorescent images confirmed that UBE2V1 was predominantly localized in the cytoplasm across all stages, with a pronounced

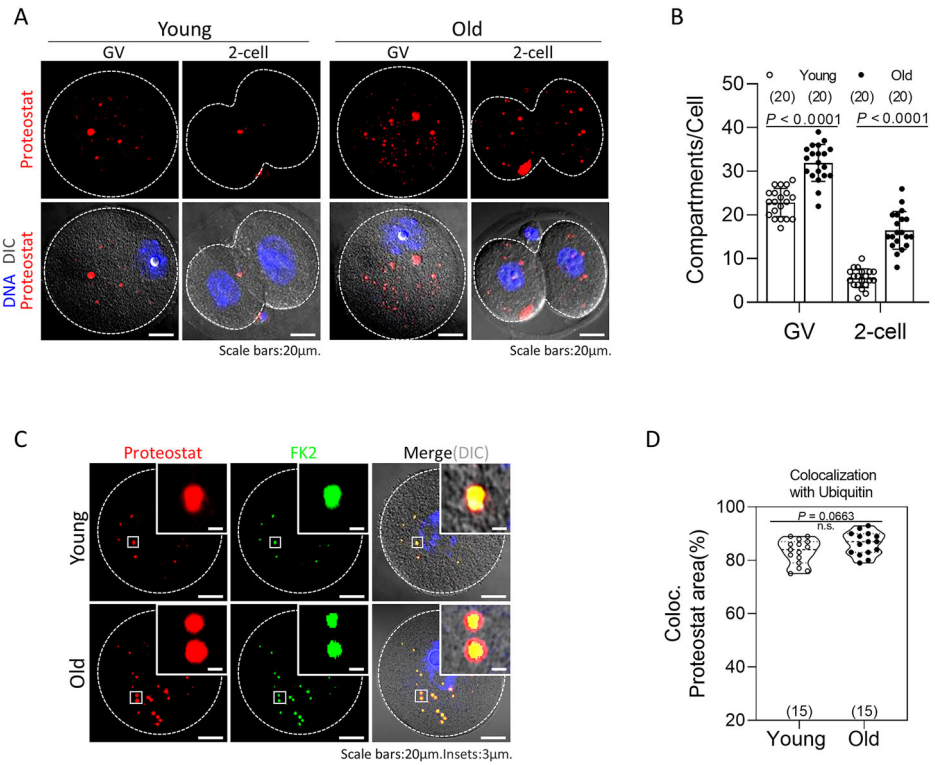

Fig. 1 | Increased ELVAs formation in oocytes and embryos from aged mice. A Confocal images of young (7–8 weeks) and old (42–45 weeks) oocytes (GV), and early embryos (2-cell) labeled with Proteostat (red) and counterstained with Hoechst33342 to visualize DNA (blue). **B** Quantification of the number of the Proteostat compartments. **C** Confocal images of young and aged mouse oocytes immunolabeled with Proteostat and anti-ubiquitin conjugates FK2. **D** Colocalization of ubiquitin and Proteostat in the experiment shown in (**C**). The total number of oocytes analyzed is indicated in the figures. Data were presented as mean ± SD. Statistical analysis was performed using an unpaired two-tailed Student's *t*-test for (**D**), and one-way ANOVA followed by multiple comparisons for (**C**). A *P*-value < 0.05 was considered statistically significant.

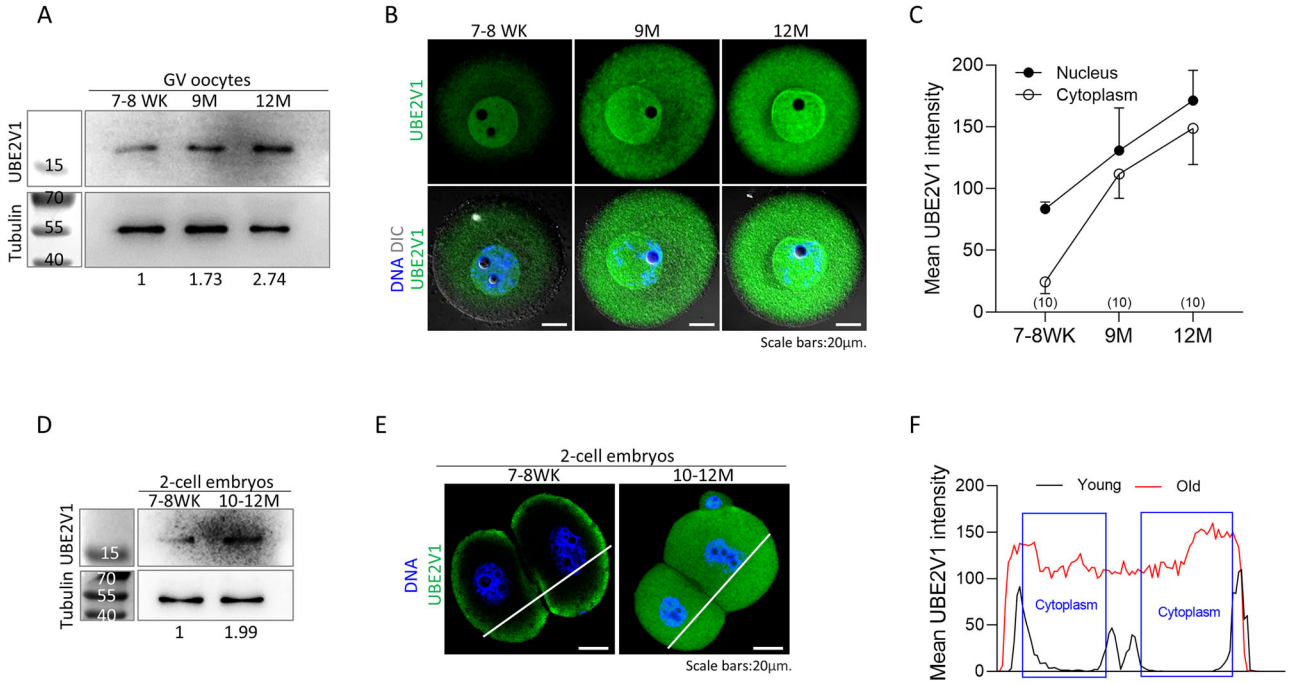

Fig. 2 | Age-related increase of UBE2V1 level. A Western blot analysis of UBE2V1 protein levels in mouse oocytes from different age groups: 7–8 weeks, 9 months, and 12 months. 100 GV oocytes per sample. **B** Representative images showing UBE2V1 localization in GV oocytes of different age groups. Oocytes from 7 to 8 weeks, 9 months, and 12 months old mice were immunostained for UBE2V1 (green) and stained with Hoechst 33342 for DNA (blue). **C** Quantitative analysis of UBE2V1 intensity in the nucleus and cytoplasm. **D** Western blot analysis of UBE2V1 protein levels in young and old 2-cell embryos, 100 embryos per sample. **E** Representative immunofluorescence images showing UBE2V1 localization in 2-cell embryos from two groups. Embryos were immunostained with anti-UBE2V1 antibody (green) and counterstained with Hoechst 33342 for nuclear DNA visualization (blue). **F** UBE2V1 intensity profiles along embryo axes (white lines in **E**) were quantified. The total number of oocytes analyzed is indicated in the figures. Data were presented as mean ± SD.

concentration in the germinal vesicle (nucleus) at the GV stage and an enrichment at the cortex in 2-cell embryos. A comparable distribution of Myc-UBE2V1, as detected by anti-Myc immunostaining in 2-cell embryos overexpressing Myc-*Ube2v1*, validated the specificity of the UBE2V1 antibody (Supplementary Fig. 2B).

We subsequently assessed UBE2V1 protein expression in GV oocytes from three different age groups using western blotting and found an age-dependent increase in UBE2V1 protein expression (Fig. 2A). Immunofluorescent staining of GV oocytes from different age groups further demonstrated a significant increase in UBE2V1 fluorescence intensity in both the cytoplasm and nucleus with aging. Notably, UBE2V1 accumulation was more prominent in the cytoplasm than in the nucleus (Fig. 2B, C). Similarly, increased UBE2V1 expression was also evident in 2-cell embryos from aged mice (Fig. 2D). In stark contrast to the cortical distribution observed in the young embryos, the aging group exhibited a uniform cytoplasmic distribution (Fig. 2E, F). Collectively, these data reveal the age-dependent upregulation and cytoplasmic distribution of UBE2V1 during oocyte aging.

UBE2V1 modulates ELVAs formation in oocytes

Having established the correlation between UBE2V1 expression and ELVAs in aged oocytes, we next test the effects of UBE2V1 more directly. To this end, we manipulated UBE2V1 expression using *Ube2v1*-specific siRNA for knockdown (UBE2V1-KD) and cRNA encoding the full-length *Ube2v1* for overexpression (UBE2V1-OE) (Fig. 3A). The efficiency of UBE2V1 knockdown (UBE2V1-KD) and overexpression (UBE2V1-OE) was confirmed by immunoblotting (Fig. 3B).

Proteostat staining revealed that UBE2V1 overexpression significantly increased, whereas its knockdown reduced, Proteostat signals in oocytes (Fig. 3C, D), indicating the regulatory role of UBE2V1 in ELVAs formation. UBE2V1 has been reported to regulate protein aggregation via K63-linked ubiquitination[12]. Consistent with this, K63-ubiquitinated proteins were significantly elevated in young oocytes (7–8 weeks) overexpressing UBE2V1 compared to controls. Furthermore, as UBE2V1 expression was found to be upregulated in old oocytes, increased levels of K63-ubiquitinated proteins were also observed in oocytes from old females (10–12 months) (Fig. 3E). More importantly, overexpression of UBE2D3, a highly expressed E2 in oocytes as we previously described[18], led to a significant reduction in both K63-linked ubiquitination and protein aggregation in oocytes (Fig. 3F–I), suggesting a potential antagonistic relationship between K48 and K63 ubiquitination, and highlighting the pivotal role of K63-linked ubiquitination in protein aggregation. Collectively, our findings identify UBE2V1 as a potentially unique E2 enzyme that promotes ELVAs formation in oocytes through a K63-linked ubiquitination mechanism.

Bidirectional roles of UBE2V1 in regulating oocyte quality

Given that oocytes sequester harmful proteins into aggregates at the GV stage and degrade them during maturation to maintain oocyte quality[14], it is plausible that alteration in protein aggregates resulting from UBE2V1 knockdown or overexpression could compromise oocyte competence. To test this hypothesis, we monitored oocyte maturation in vitro (Fig. 4A). Although neither UBE2V1 depletion nor overexpression affected meiotic resumption, both conditions significantly impaired first polar body (PB1) extrusion after 14 h of culture compared to controls (Fig. 4B, C), indicating disrupted meiotic progression. Further, we examined meiotic spindle morphology and chromosome alignment by immunostaining with α-tubulin. Most control oocytes displayed a typical barrel-shaped spindle and well-aligned chromosomes at the metaphase plate. In contrast, ~45% of UBE2V1-OE oocytes and ~60% of UBE2V1-KD oocytes exhibited abnormal spindle structures (Fig. 4D, E, arrows) and misaligned chromosomes (Fig. 4D, E, arrowheads). Given the established link between chromosome misalignment and aneuploidy [19], we performed chromosome spread analysis. While the majority of control oocytes maintained euploidy with 20 univalent chromosomes, 33% of oocytes overexpressing UBE2V1 were

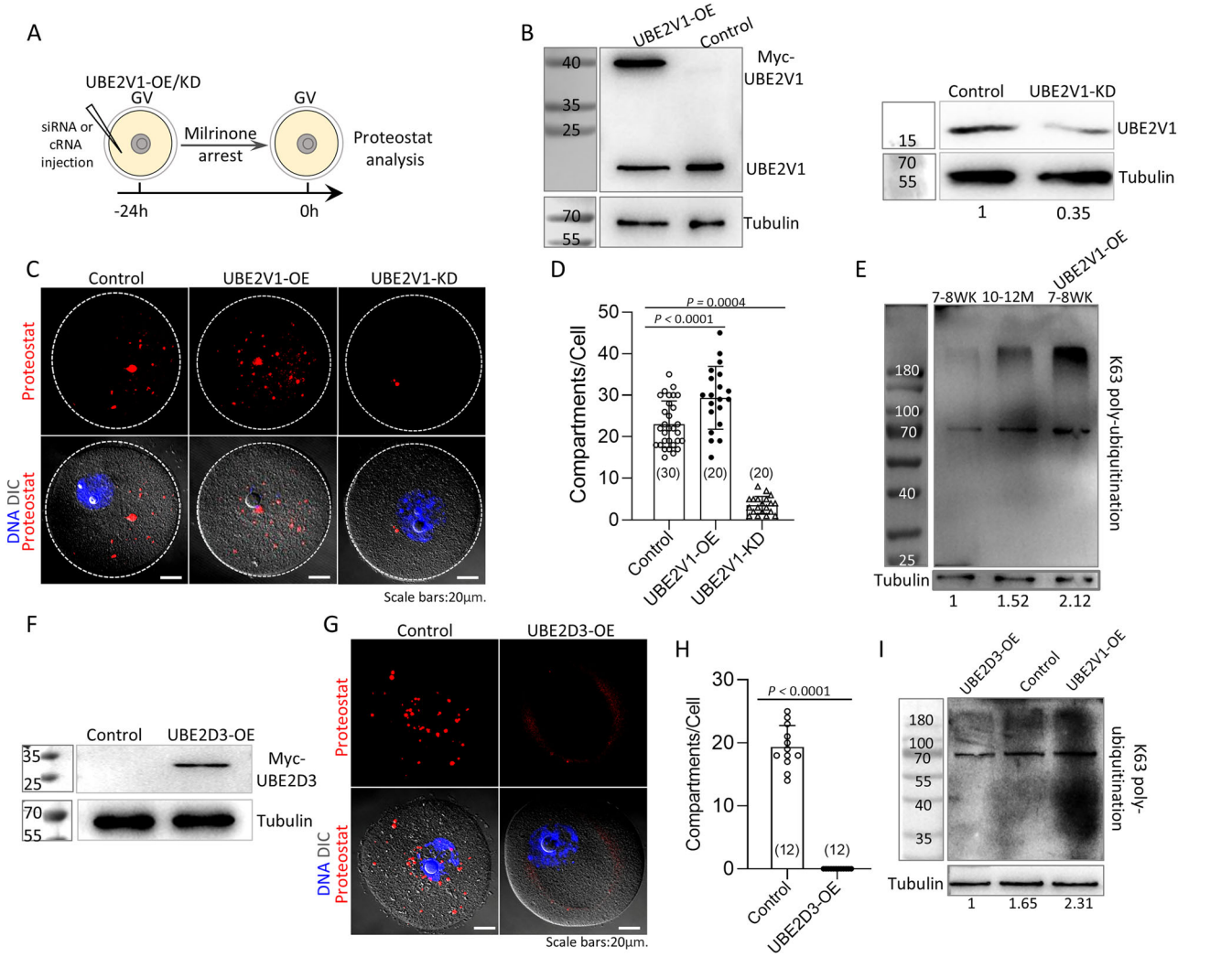

Fig. 3 | UBE2V1 favors ELVAs formation. A Schematic diagram of the UBE2V1 overexpression and knockdown experiment in oocytes. **B** Validation of exogenous Myc-UBE2V1 overexpression and UBE2V1 knockdown efficiency in oocytes. Western blot analysis was performed using anti-UBE2V1 antibody to confirm exogenous Myc-UBE2V1 mRNA overexpression and siRNA-mediated UBE2V1 depletion in GV oocytes. Tubulin was used as a loading control. Protein lysates from 100 GV oocytes were loaded per lane. **C** Confocal images of control (7–8 weeks), UBE2V1 overexpression (UBE2V1-OE), and UBE2V1 knockdown (UBE2V1-KD) oocytes at the GV stages labeled with Proteostat (red). **D** Quantification of the number of the Proteostat compartments. **E** Western blot analysis of K63 poly-ubiquitination protein levels in Young (7–8 weeks), Old (42–45 weeks), and Young with UBE2V1 overexpression oocytes. Tubulin was used as a loading control. Total proteins from 80 oocytes were loaded in each lane. **F** Western blot analysis was performed using anti-Myc antibody to confirm the overexpression of Myc-UBE2D3 mRNA. **G** Confocal images of control (7–8 weeks) and UBE2D3-overexpressing (UBE2D3-OE) oocytes at the GV stage labeled with Proteostat (red) and counterstained with Hoechst 33342 for nuclear DNA visualization (blue). **H** Quantification of the number of the Proteostat compartments. **I** Western blotting analysis of K63 polyubiquitinated protein in UBE2D3-OE, control and UBE2V1-OE oocytes. Tubulin was used as a loading control. Protein lysates from 90 GV oocytes were loaded per lane. The total number of oocytes analyzed is indicated in the figures. Data were presented as mean ± SD. Statistical analysis was performed using an unpaired two-tailed Student's *t*-test for (**H**), and one-way ANOVA followed by multiple comparisons for (**D**). A *P*-value < 0.05 was considered statistically significant.

aneuploid (Supplementary Fig. 3). These results highlight the bidirectional and dosage-sensitive roles of UBE2V1 in regulating oocyte quality.

UBE2V1 overexpression leads to protein aggregation and developmental defects in embryos

Given the observed association between UBE2V1 upregulation and increased protein aggregation in aging embryos, we next examined the impact of UBE2V1 overexpression on early embryo development. MII oocytes were injected with *Ube2v1* cRNAs prior to IVF, and the resulting embryos were analyzed (Fig. 5A). As expected, Proteostat signals were markedly increased in 2-cell embryos after UBE2V1 overexpression (Fig. 5B). Remarkably, the developmental rate of UBE2V1-OE embryos began to decline after the first cleavage with only 40% of cleaved embryos successfully developing to the blastocyst stage after 4 days culturing (Fig. 5C, D).

Given the importance of DNA damage repair and major zygotic genome activation (ZGA) during preimplantation development, we explored whether these processes were disturbed in UBE2V1-OE embryos. We analyzed γH2AX level, a well-established indicator of DNA damage, and observed a significant increase in γH2AX levels in 2-cell stage embryos following UBE2V1 overexpression (Supplementary Fig. 4A, B). Furthermore, total de novo transcripts were detected via ethynyl uridine (EU) staining[19] and showed that the overall transcriptional activation in two-cell embryos was impaired by UBE2V1 overexpression (Supplementary Fig. 4C, D). Notably, a markedly high level of γH2AX was also observed in blastocyst embryos with UBE2V1 overexpression, indicating persistent damage throughout preimplantation embryo development (Fig. 5E, F). In conclusion, these findings suggested a causal role of enhanced UBE2V1 expression in compromising the developmental competence of embryos.

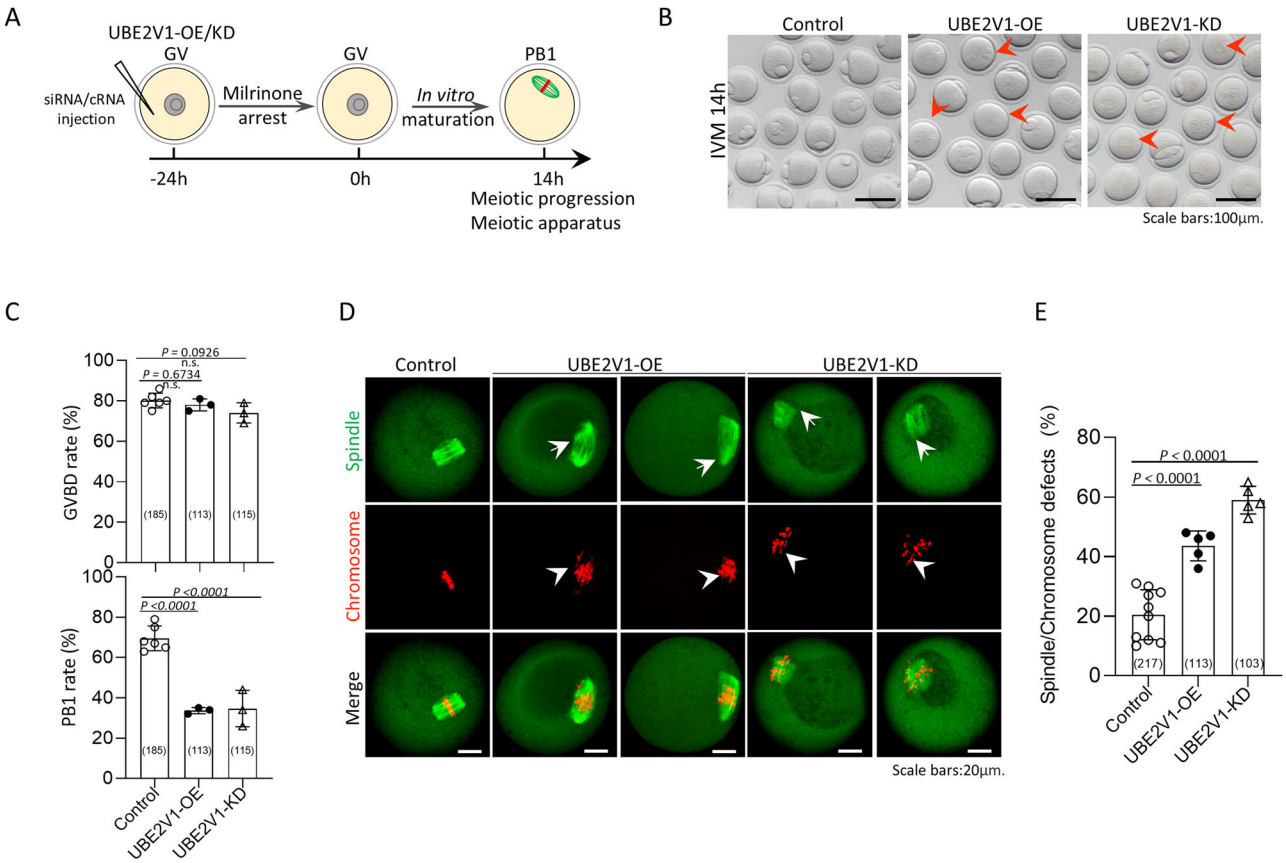

Fig. 4 | Bidirectional roles of UBE2V1 in oocyte meiosis. A Schematic diagram of the UBE2V1 overexpression and knockdown experiment in oocytes. **B** Phase-contrast images of oocytes from the control, UBE2V1-OE, and UBE2V1-KD after in vitro matured for 14 h. **C** Quantitative analysis of GVBD and PB1 extrusion rates in control, UBE2V1-OE, and UBE2V1-KD. **D** Control, UBE2V1-OE, and UBE2V1-KD oocytes were stained with a-tubulin antibody to visualize the spindle (green) and counterstained with PI to visualize chromosome (red). Control metaphase oocytes present a typical barrel-shape spindle and well-aligned chromosomes. Spindle defects (arrowheads) and chromosome misalignment (arrow) were frequently observed in UBE2V1-OE and UBE2V1-KD oocytes. **E** Quantification of the spindle/chromosome defects in each group. Data are means ± SD, and statistical analyses were performed with one-way ANOVA followed by multiple comparisons. A *P*-value < 0.05 was considered statistically significant. The total number of analyzed oocytes (from at least three independent experiments) is indicated in each graph.

UBE2V1 overexpression mimics the subcellular phenotypes observed in aged oocytes

We further compared the effects of maternal aging and UBE2V1 overexpression at the subcellular level in oocytes, with a particular focus on the biological consequence of protein aggregation (Fig. 6A). We first assessed mitochondrial distribution and function, given the established link between protein aggregation and mitochondrial dysfunction[20]. Mito Tracker staining and confocal scanning revealed that most young GV oocytes showed a typical perinuclear mitochondrial distribution (Fig. 6B). However, approximately 50% of oocytes from aged mice exhibited abnormal mitochondrial clustering, a defect that was significantly exacerbated by UBE2V1 overexpression in young oocytes (Fig. 6B, C). Since mitochondria are the primary site of intracellular ROS production, and mitochondrial dysfunction is known to contribute to age-related fertility decline due to redox imbalances[21], we measured ROS levels. Aged oocytes displayed significantly elevated ROS levels compared to young controls, and UBE2V1 overexpression in young oocytes similarly led to a marked increase in ROS signals (Fig. 6D, E). Additionally, mitochondrial membrane potential (MMP), a key indicator of mitochondrial function, was significantly decreased in both aged oocytes and young oocytes with UBE2V1 overexpression (Fig. 6F, G).

Protein aggregates can disrupt the protein synthesis environment via induction of ER stress[22]. In oocytes, following meiotic resumption, localized protein synthesis, particularly in regions near chromosomes, is crucial for proper spindle assembly, chromosome alignment, and segregation[23]. Using O-propargyl-puromycin (OPP), a specific covalent label of growing polypeptides[24], we analyzed nascent protein synthesis in MI oocytes. our results demonstrated that the whole oocyte was translationally active with two distinct areas-chromosomal and perispindular areas-showing increased activity. Remarkably, a significant decrease in translation fluorescence signal was observed in Old and Young+OE oocytes, particularly in these hot spot regions (Fig. 6H, I). In conclusion, these findings suggest that excessive UBE2V1 expression replicates the subcellular phenotypes seen in aged embryos.

Restoring UBE2V1 expression ameliorates defects in protein aggregation and meiosis of aged oocytes

Having established a causal link between elevated UBE2V1 expression, protein aggregation and decline in oocyte quality, we next sought to determine whether restoring UBE2V1 expression in aged oocytes could ameliorate age-related defects. To explore this, we microinjected siRNA targeting UBE2V1 into aged GV oocytes (hereafter referred to as Old+KD) (Fig. 7A). After optimizing the siRNA incubation period, we found that UBE2V1 protein levels in aged oocytes were reduced to levels comparable to those in young oocytes 18 h post-siRNA injection (Fig. 7B). Remarkably, the increased ELVAs formation typically seen in aged oocytes was reversed in Old+KD oocytes (Fig. 7C, D), further underscoring the crucial role of UBE2V1 in driving age-related protein aggregation in oocytes.

To examine the biological consequence, we evaluated meiotic progression, spindle organization and chromosome alignment and segregation (Fig. 7A). Statistical analysis demonstrated an improvement in meiotic progression, as revealed by the increased PB1 extrusion rate in Old+KD

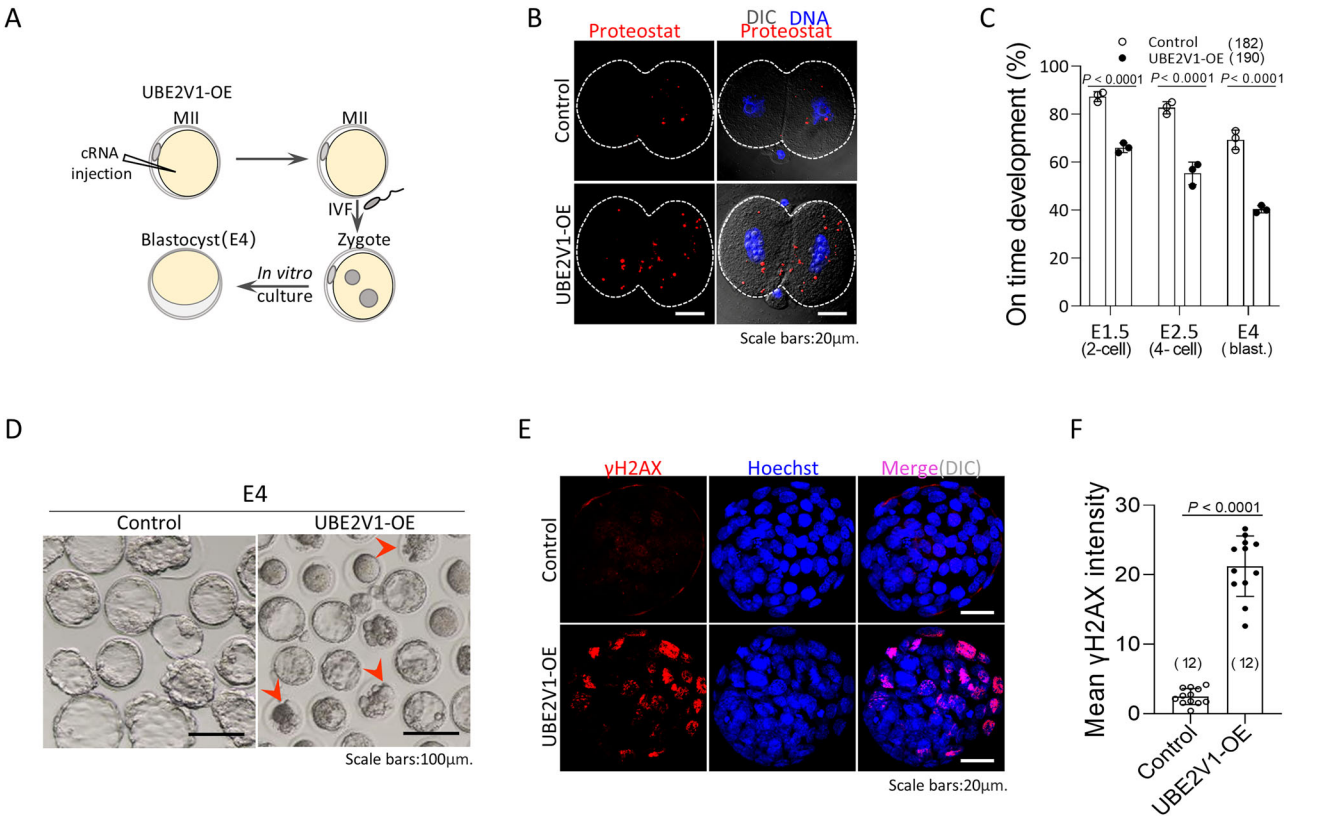

Fig. 5 | UBE2V1 overexpression leads to protein aggregation and developmental defects in embryos. A Schematic illustration of the UBE2V1 overexpression experiments in mouse embryos. **B** Confocal images of control and UBE2V1 overexpression (UBE2V1-OE) 2-cell embryos labeled with Proteostat (red). DNA was counterstained with Hoechst33342 (blue). **C** Quantification of embryo development rates at E1.5, E2.5, and E4 days from the control and UBE2V1-OE groups. **D** Phase-contrast images of E4 embryos. The arrows indicate embryos experiencing cytoplasmic fragmentation and developmental arrest. **E** γH2AX staining was used to assess blastocyst apoptosis in blastocyst embryos derived from the control and UBE2V1-OE groups. **F** The mean fluorescence intensity of γH2AX in the control and UBE2V1-OE was quantified. The total number of oocytes analyzed per condition is indicated in each graph. Data were presented as mean ± SD of three independent experiments. Statistical analysis was performed using an unpaired two-tailed Student's *t*-test for (**F**), and multiple *t*-test for (**C**). A *P*-value < 0.05 was considered statistically significant.

oocytes (Fig. 7E). Moreover, defects in spindle organization and chromosome alignment were also partially alleviated in Old+KD oocytes (Supplementary Fig. 5A, B). Finally, the high incidence of aneuploidy exhibited in old oocytes was rescued to a level comparable to that in young oocytes (Supplementary Fig. 5C, D). These results collectively suggest that restoring UBE2V1 expression can rescue age-related protein aggregation and meiotic defects.

UBE2V1 depletion mitigates protein aggregation and developmental defects in aged embryos

We next asked whether reducing UBE2V1 expression in old embryos could ameliorate the observed developmental defects. To test this, we injected siRNA targeting UBE2V1 into MII oocytes from aged mice and subjected them to IVF. After fertilization, we assessed protein aggregation levels and embryo development (Fig. 8A). Notably, UBE2V1 knockdown (Old+KD embryos) resulted in a significant reduction in protein aggregates in 2-cell stage embryos compared to the untreated old embryos (Fig. 8B). Consistently, the resulting embryos also displayed a higher rate of successful development to the blastocyst stage (Fig. 8C). Importantly, defects in DNA damage repair and embryonic genomic activation that observed in old embryos were ameliorated in Old+KD embryos (Supplementary Fig. 6). In addition, lysosomal activity, which was reduced in aged oocytes, was restored to levels comparable to those in young controls following UBE2V1 knockdown (Fig. 8D, E). DNA damage, as assessed by γH2AX staining, was also significantly reduced in blastocysts derived from the Old+KD group (Fig. 8F, G). Furthermore, post-implantation outcomes were improved, as evidence by a higher live pup rate following embryo transfer at E18.5 (Fig. 8H).

Together, these findings indicate that restoring UBE2V1 expression in aged embryos alleviates protein aggregation and improves developmental competence, highlighting UBE2V1 as a potential therapeutic target for age-related female fertility decline.

Discussion

Dysfunction in protein homeostasis is a hallmark of many age-related diseases, most notably neurodegenerative disorders[25]. Beyond neurons, age-related protein inclusions have also been observed in tissues such as the heart[26], muscle fibers[27], and endothelial cell[28]. Oocytes, some of the longest-lived cells in the body, exhibit well-documented quality decline with age in mammals[29]. Notably, the recent discovery of protein aggregates in oocytes highlights a previously unexplored aspect of oocyte aging[14,30]. However, the effects of maternal aging on proteostasis in mouse oocytes and the underlying molecular mechanisms remain largely elusive.

Given the observed aggregation of ubiquitinated protein in aged oocytes, we examined the expression profiles of E2 ubiquitin-conjugating enzymes in oocytes from young and old mice and identified an age-dependent increase in UBE2V1 protein levels (Fig. 2). Notably, UBE2V1 has been shown to promote protein aggregation through K63-linked ubiquitination in cardiomyocytes[12]. Generally, E2 enzymes determine the type of ubiquitination modification to occur. Among the seven lysine residues in ubiquitin (K6, K11, K27, K29, K33, K48, and K63), K48-linked chains target proteins for proteasomal degradation, whereas the K63-linked

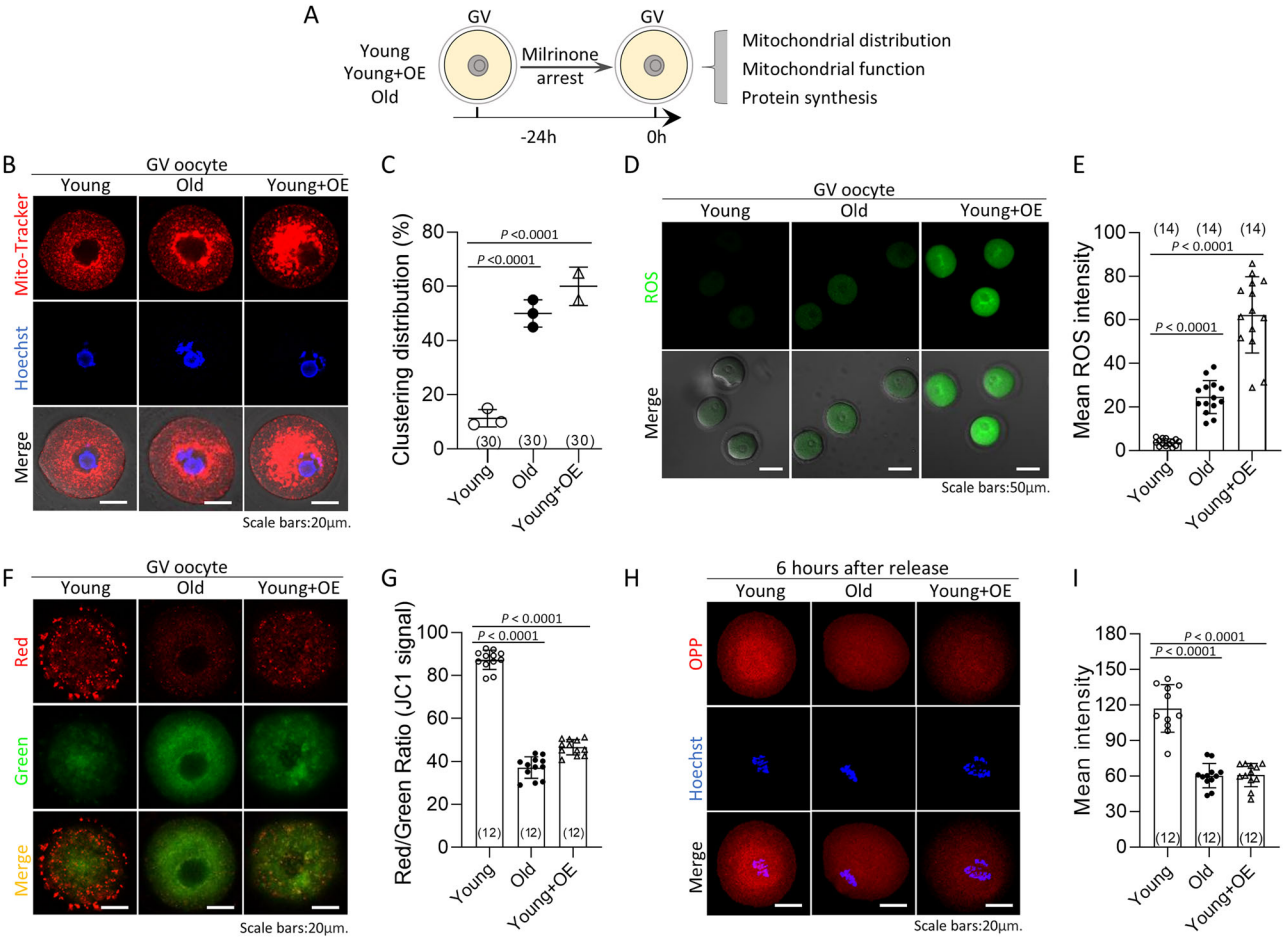

Fig. 6 | UBE2V1 overexpression mimics the subcellular phenotypes observed in aged oocytes. A Schematic diagram of experimental design of subcellular phenotypic analysis. **B** Confocal images showing mitochondrial distribution in the Young, Old, and Young+OE groups. **C** Quantification of the proportion of oocytes with clustering mitochondria distribution (arrows). **D** Confocal images of ROS level in Young, Old, and Young+OE groups. **E** Quantitative analysis of the ROS fluorescence intensity in Young, old, and Young+OE groups. **F** Mitochondrial membrane potential in Young, Old, and Young+OE oocytes was evaluated using JC-1 staining. Green fluorescence indicates inactive mitochondria, while red fluorescence indicates active mitochondria in the oocytes. **G** Histogram showing the JC-1 red/green ratio. **H** Confocal images of Young, old, and Young+OE oocytes (at 6 h after release for each group) labeled with OPP (conjugated with AF594, red) to indicate new protein synthesis levels, with DNA counterstained using Hoechst 33342 (blue). **I** Statistical analysis of the OPP fluorescence intensity in Young, Old, and Young+OE. Throughout, data are presented as means ± SD, and one-way ANOVA followed by multiple comparisons was used for statistical analysis. A *P*-value < 0.05 was considered statistically significant. The total number of oocytes analyzed (from at least three independent experiments) is indicated in each graph.

ubiquitination serves as a molecular platform for protein/protein interaction important for kinase signaling activation, receptor endocytosis, protein trafficking, and DNA damage repair[31]. In this work, we found that the dynamic expression of UBE2V1 protein correlates with aggresome formation-showing significantly accumulation at GV stage, followed by a marked decline after fertilization. Through loss- and gain-of function experiments, we provide direct evidence that UBE2V1 positively regulates protein aggregation in oocytes. Consistent with the report described previously[12], K63-linked ubiquitination were increased after UBE2V1 overexpression, and reduced following knockdown. Importantly, overexpression of UBE2D3, another E2 that catalyzes K48-linked ubiquitination, led to a significant reduction in both K63-linked ubiquitination and protein aggregation in oocytes (Fig. 3F, H). These findings suggest that UBE2V1 may be a previously undefined regulator of ELVAs formation in oocytes through K63-linked ubiquitination. However, the detail molecular mechanism underlying this process warrants further exploration.

2-cell embryos from old mice also exhibited elevated UBE2V1 expression, increased protein aggregation, and impaired embryonic development. Interestingly, deleting UBE2V1 significantly alleviated protein aggregation and developmental defects in aged embryos. Notably, lysosomal activity was reduced in aged embryos but was rescued by UBE2V1 knockdown. These findings suggest that UBE2V1-induced protein aggregation may overwhelm the degradative capacity of the autophagy–lysosome system, thereby contributing to impaired clearance and further decline in cellular proteostasis. We propose that this feed-forward loop plays a key role in the deterioration of autophagic activity and embryonic developmental potential in aged mice.

ELVAs formation is required for detrimental protein degradation, which is crucial for preserving oocyte quality[14]. In line with this, reduced ELVAs formation resulting from UBE2V1 depletion led to the production of defective oocytes. Defective developmental competence was also observed in oocytes with excessive protein aggregation, such as in UBE2V1-overexpressing and aged oocytes (Figs. 4 and 5). One possible explanation is that the accumulation of protein aggregates may overwhelm the degradative capacity of the endolysosomal system, thereby contributing to proteotoxic stress. Consistent with this notion, defective in mitochondrial distribution and function, as well as impaired protein synthesis, were also observed in UBE2V1-overexpressing and aged oocytes. ROS, not only destroys DNA, but also disrupts the protein synthesis environment, which causes more serious consequences such as protein synthesis error and aggregates accumulation, creating a vicious circle. Importantly, temporal and spatial regulation of translation ensures that proteins are synthesized at the right time

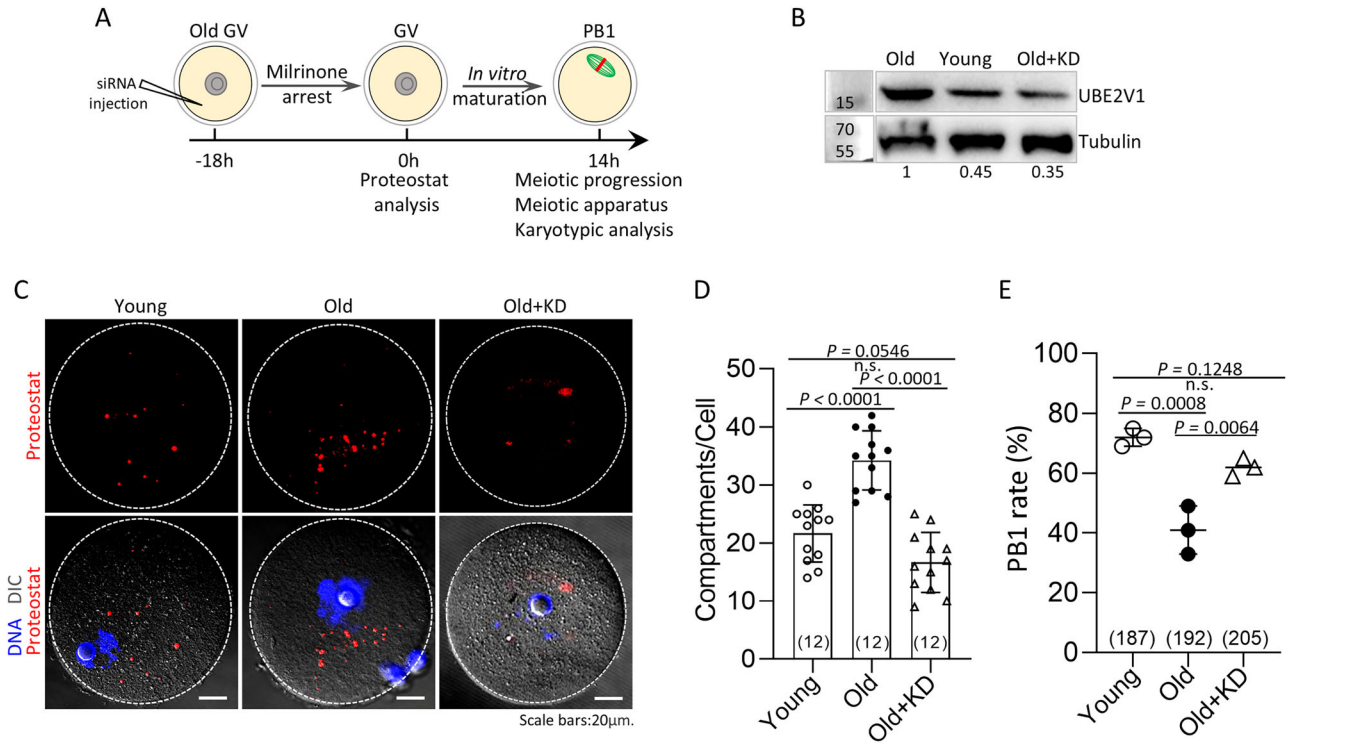

Fig. 7 | Restoration of UBE2V1 expression alleviates protein aggregation and meiotic defects in aged oocytes. A Schematic representation of the UBE2V1 knockdown experiments in old oocytes. **B** Western blot analysis showing knockdown efficiency of UBE2V1 siRNA. Total proteins from 100 oocytes were loaded in each lane. **C** Confocal images of Young (7–8 weeks), Old (42–45 weeks), and UBE2V1 knockdown (Old+KD) oocytes at GV stage labeled with Proteostat (red). **D** Quantification of the number of the Proteostat compartments. **E** Quantitative analysis of Pb1 extrusion rates in Young, Old, and Old+KD groups. Data were expressed as mean ± SD of at least three independent experiments, and one-way ANOVA followed by multiple comparisons was used for statistical analysis. A *P*-value < 0.05 was considered statistically significant. Oocytes analyzed in each group was indicated in each figure.

and in the appropriate locations within the oocyte and embryo, which is essential for processes such as spindle assembly, chromosome alignment[23] and zygotic genome activation[32,33]. Although these effects may stem from protein aggregation, we cannot exclude the possibility that UBE2V1 regulates these processes through alternative mechanisms, especially considering the diverse cellular functions mediated by K63-linked ubiquitination[31].

In summary, our findings underscore the critical roles of UBE2V1 in oocyte aging, and suggest additional ways for developing targeted therapies to improve reproductive outcomes in aged females.

Materials and methods

Mice

ICR mice were used in this study. 7–8-week-old female mice were used as a control. To generate a natural aging mouse model, 10–12-month-old female mice which near the end of their reproductive lifespan were used. We have complied with all relevant ethical regulations for animal use, and all experiments were approved by the Animal Care and Use Committee of Nanjing Medical University and were performed in accordance with institutional guidelines.

Antibodies

The following antibodies were purchased: Rabbit Polyclonal UEV1A antibody (Cat#: GTX16444; Gene Tex); Mouse monoclonal [3F2] to gamma H2A.X (Cat#: ab22551; Abcam); Human anti-centromere CREST antibody (Cat#: 15234; Antibodies Incorporated); Cy5-conjugated donkey anti-human IgG (Cat#: 709605149 and 705095147; Jackson Immuno-Research Laboratory); Horseradish peroxidase (HRP) conjugated goat anti-rabbit (Cat#: SA00001-2) and IgG LC3 Polyclonal antibody (Cat#: 14600-1-AP) (Protein Tech); FITC-conjugated goat anti-rabbit IgG (Cat#: A31627; Thermo Fisher). Mouse monoclonal FK2 primary antibodies (Cat#: ST1200), Mouse monoclonal FITC conjugated anti α-tubulin antibody (Cat#: F2168), FITC conjugate goat anti-mouse IgG Antibody (Cat#: F0257), TRITC conjugate Goat Anti-Mouse IgG Antibody (Cat#: AP124R), Rabbit Monoclonal Anti-Ubiquitin (Lys63-Specific) Antibody (Cat#: 05-1308), and Hoechest33342 (Cat#: B2261) were purchased from Sigma.

Oocyte collection and culture

To obtain fully grown GV oocytes, mice were superovulated with an intraperitoneal injection of 5 IU pregnant mare serum gonadotropin (PMSG). Cumulus-enclosed oocytes were isolated 46–48 h later, and the cumulus cells were removed by repeated pipetting to obtain denuded oocytes. The oocytes were cultured in drops of M2 medium covered with mineral oil at 37 °C under 5% CO_2. For the collection of ovulated MII oocytes, mice were superovulated with PMSG followed by an injection of 5 IU human chorionic gonadotropin (HCG). Cumulus–oocyte complexes were isolated from the oviducts, and cumulus cells were removed by incubation with 1 mg/mL hyaluronidase.

In vitro fertilization and embryo transfer

IVF assays were conducted according to protocol[34] with minor modifications. In brief, sperm were collected from the cauda epididymis of ICR mice aged 10–20 weeks and left to capacitate for 1 h in HTF fertilization medium (Millipore, Merck) supplemented with 10 mg/ml BSA. The capacitated spermatozoa were then added to HTF drops containing denuded oocytes, as previously described[35]. After an appropriate co-incubation period at 37 °C, the presumptive zygotes were washed to remove excess sperm. Then, zygotes were transferred to KSOM medium (Millipore, Merck) and incubated up to the blastocyst stage at 37 °C in a humidified atmosphere of 5% CO_2, 5% O_2, and 90% N_2.

For the embryo transfer experiments, 2-cell stage embryos were transferred into the oviducts of pseudopregnant ICR female mice at a ratio

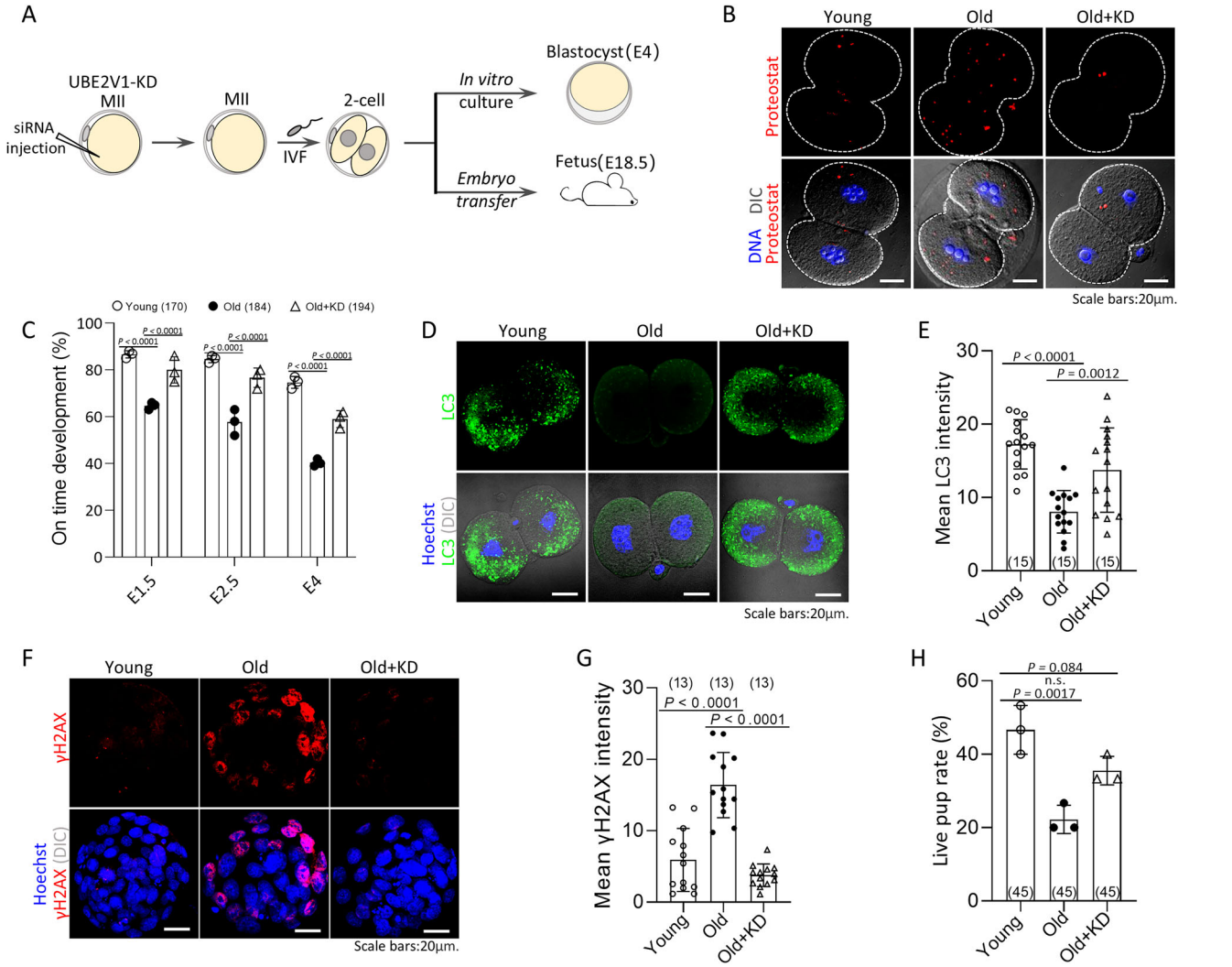

Fig. 8 | UBE2V1 depletion rescues age-related embryonic defects. A Schematic diagram showing the rescue experiments in embryos. **B** Confocal sections of Young, Old, and Old+KD embryos at the 2-cell stages labeled with Proteostat. Proteostat (red), and DNA was counterstained with Hoechst33342 (blue). **C** Quantification of embryo development rates at E1.5, E2.5, and E4 days from the Young, Old, and Old+KD groups. **D** Representative images showing LC3 (green) and Hoechst 33342 (blue) staining in the Young, Old, and Old+KD groups. **E** Mean LC3 fluorescence intensity in the Young, Old, and Old+KD groups. **F** γH2AX staining was used to assess blastocyst apoptosis in 2-cell embryos derived from the Young, Old, and Old+KD groups. γH2AX (rad) was detected, and DNA was counterstained with Hoechst 33342 (blue). **G** The mean fluorescence intensity of γH2AX in the Young, Old, and Old+KD was quantified. **H** Statistical Analysis of Live Birth Rate at E18.5 Following Embryo Implantation. The total number of oocytes analyzed per condition is indicated in each graph. Data were presented as mean ± SD of three independent experiments. Statistical analysis was performed using one-way ANOVA followed by multiple comparisons for (**E**, **G**, and **H**), and multiple *t*-test for (**C**). A *P*-value < 0.05 was considered statistically significant.

of 15 embryos per recipient. Surrogate mothers were sacrificed at embryonic day 18.5 (E18.5) to evaluate fetal development.

Plasmid construction and cRNA synthesis

Total RNA was extracted from 50 oocytes using the Arcturus PicoPure RNA Isolation Kit (KIT0204; Applied Biosystems), and cDNA was generated using the Quantitect Reverse Transcription kit (205,311; Qiagen). Plasmid construction and cRNA synthesis were performed as described previously[36]. Purified PCR products were digested with EcoRI and Xba1 (R3101S and R0145S, NEB), and then cloned into the pCS2+ vector with Myc tags. For mRNA synthesis, plasmids were linearized with NotI, followed by in vitro transcription using the SP6 mMESSAGE mMACHINE kit (AM1340; Thermo Fisher) according to the manufacturer's instructions. The cRNA was then purified using the RNeasy Micro Kit (74004; Qiagen). Synthesized cRNA was aliquoted and stored at −80 °C. The related primer sequences can be found in Supplementary Table 1.

Overexpression and knockdown experiments

To achieve overexpression and knockdown in mouse oocytes, microinjection was performed employing an inverted microscope (Eclipse Ti-S, Nikon) equipped with a micromanipulator (Narishige). siRNA duplexes targeting *Ube2v1* were obtained from Gene Pharma and prepared as 20 μmoL/L stock solutions. For knockdown analysis, 2.5 pL of *Ube2v1* siRNA (1 mM) or an equivalent volume of negative control siRNA was microinjected into oocytes. For overexpression experiments, 10 pL of cRNA (10 ng/μL) was introduced into GV-stage oocytes, with PBS injection serving as the control. Following injections, oocytes were arrested at the GV stage in M2 medium containing 2.5 μM milrinone for 24 h to facilitate siRNA or cRNA working. To overexpress or knockdown *Ube2v1* in embryos, 5–10 pL of cRNA or siRNA were injected into MII before fertilization. After fertilization, zygotes were cultured in fresh KSOM medium under mineral oil in a 5% CO_2 incubator at 37 °C for subsequent development. The related sequences can be found in Supplementary Table 1.

Quantitative real-time PCR

Total RNA was extracted from 50 oocytes using Arcturus PicoPure RNA Isolation Kit (Applied Biosystems, CA, USA). First-strand cDNA was synthesized with the cDNA Synthesis Kit (Qiagen, Germany). Real-time PCR was conducted with SYBR Green dye on an ABI StepOnePlus Real-time PCR system (Applied Biosystems, CA, USA). Glyceraldehyde-3-phosphate dehydrogenase (Gapdh) served as the internal control. Each experiment was performed in triplicate or more. The related primer sequences can be found in Supporting Information Supplementary Table 1.

Immunofluorescence and confocal microscopy

Oocytes or embryos were fixed with 4% paraformaldehyde for 30 min and then permeabilized with 0.5% Triton X-100 for 20 min. After blocking in 1% BSA in PBS for 1 h, samples were incubated overnight at 4 °C with primary antibodies: anti-UBE2V1 antibody, anti-gamma H2A.X antibody, anti-LC3 antibody or anti-tubulin antibody (diluted in 1% BSA). After three washes for 5 min each, the oocytes or embryos were labeled with secondary FITC-or TRITC -conjugated antibody (diluted in 1% BSA) for 1 h at room temperature. Following three washes, the oocytes or embryos were stained with Hoechst 33342 for 20 min to visualize the chromosomes. Finally, the oocytes were mounted on microscope slides and examined using a laser scanning confocal microscope (LSM 700, Zeiss).

For Proteostat staining (PROTEOSTAT® Aggresome detection kit; Cat#: ENZ-51035-0025; ENZO), oocytes and embryos were processed according to the manufacturer's instructions. Briefly, Cells were fixed with 2% formaldehyde in 1× Assay Buffer containing 0.05% BSA for 1 h at room temperature (RT), followed by permeabilization in 1× Assay Buffer with 0.5% Triton X-100 and 3 mM EDTA for 1 h on ice. The samples were then washed in PBS with 0.05% BSA, immunolabeled with primary antibodies (FK2) for 1 h at RT in 1× Assay Buffer with 0.05% BSA, and washed again in PBS with 0.05% BSA for 1 h at RT. The cells were then incubated with secondary antibodies (FITC-conjugated goat anti-mouse IgG) and Proteostat (1:2000) for 1 h at RT in 1× Assay Buffer with 0.05% BSA. After a final wash in PBS with 0.05% BSA, the samples were prepared for imaging as described. DNA was counterstained with Hoechst 33342, as provided in the kit.

To detect mitochondrial distribution, oocytes were cultured in M2 medium containing 200 nM Mito-Tracker Red (Molecular Probes, Eugene, OR) for 30 min at 37 °C. Chromosomes were counterstained with Hoechst 33342 for 10 min. Mitochondrial membrane potential was evaluated using Mito-Probe JC-1 Assay Kit (M34152, Thermo), oocytes were incubated in M2 medium containing 2 μM JC-1 for 30 min at 37 °C. After three washes, the samples were mounted in antifade medium (Vectashield, Vector Laboratories, CA, USA) and examined using a laser scanning confocal microscope (LSM 700, Zeiss).

Western blotting

The samples containing a sufficient number of oocytes were lysed in Laemmli buffer and incubated at 95 °C for 5 min, then frozen at −20 °C until use. Total oocyte proteins were separated by 10% SDS-PAGE and electrophoretically transferred to the PVDF membrane. The membranes were then blocked for 1 h in Tris-buffered saline with 0.1% Tween-20 (TBST) and 5% low-fat dry milk. After blocking, the membranes were incubated overnight at 4 °C with the appropriate primary antibodies (diluted in 5% low-fat dry milk). The membranes were then washed three times with PBST (PBS containing 0.1% Tween 20) and incubated for 1 h at room temperature with HRP-conjugated secondary antibodies (diluted in 5% low-fat dry milk). Protein bands were subsequently visualized using the ECL Plus Western Blotting Detection System (GE Healthcare, Little Chalfont, United Kingdom). Tubulin served as the loading control.

Chromosome spreading

Chromosome spreads were prepared following a previously described protocol[37]. Briefly, oocytes were treated with Tyrode's buffer (pH 2.5) at 37 °C for approximately 30 s to remove the zona pellucida. After a 10-min recovery period in M2 medium, the oocytes were fixed on a glass slide in a drop of 1% paraformaldehyde containing 0.15% Triton X-100. Once air-dried, the oocytes were incubated with CREST antibodies (1:500) overnight at 4 °C for kinetochore labeling, followed by a 1-h incubation with a Cy5-conjugated secondary antibody. Chromosomes were stained with Hoechst 33342, and the samples were analyzed using a laser scanning confocal microscope.

EU incorporation assays

EU incorporation assays were conducted using Click-iT RNA Imaging kits (C10329; Invitrogen). In summary, 2-cell embryos were cultured in KSOM medium with 1 mM 5-ethynyl uridine (EU) for 3 h. 2-cell embryos were fixed overnight at 4 °C in 4% paraformaldehyde. Following fixation, they were permeabilized with 0.5% Triton for 15 min at room temperature and washed three times with PBST. In a dark environment at room temperature, 2-cell embryos were then incubated in a Click-iT reaction mixture for 30 to 60 min. After incubation, they were washed twice with a washing buffer. The nucleus was stained with Hoechst 33342 diluted at 1:1000 in PBST for 15 min. Images were obtained using a confocal laser scanning microscope, and fluorescence intensity was measured as described previously. The fluorescence signal was determined by calculating the average intensity after subtracting the background.

ROS evaluation

To assess reactive oxygen species (ROS) levels, oocytes were incubated in M2 medium containing 5 μM CM-H2DCFDA (C6827; Invitrogen) at 37 °C for 30 min in a 5% CO_2 incubator. After incubation, the oocytes were washed three times and transferred to a live cell-imaging dish, covered with mineral oil. Fluorescent images were then immediately captured using a Zeiss Laser Scanning Confocal Microscope (LSM 700; Zeiss).

Protein synthesis detection

To detect nascent protein synthesis, MI stage oocytes were cultured in M2 medium supplemented with 50 μM OPP from Click-iT™ Plus OPP Alexa Fluor™ 594 Protein Synthesis Assay kits (C10457; Invitrogen) for 30 min. After a rapid wash with PBS/PVP three times, the oocytes were fixed at room temperature in 3.7% paraformaldehyde for 15 min. The oocytes were then permeabilized with 0.5% Triton at room temperature for 15 min, followed by three washes with 0.1% BSA, and then blocked in 0.1% BSA for one hour. Afterward, the oocytes were washed three times with PBST. In the dark at room temperature, the oocytes were incubated in the Click-iT OPP reaction cocktail for 30 min. Following the incubation, the oocytes were washed twice with Rinse buffer. The nuclei were stained with Hoechst 33342 diluted 1:1000 in PBST for 15 min. Finally, the samples were mounted on slides and examined using a confocal laser scanning microscope.

Quantitative analysis of confocal microscope images

Maximum intensity projection images were generated from z-stack confocal microscopy to examine ELVAs. Quantification of ELVAs was performed using the "Analyze Particles" function in FIJI. Images were first converted to 8-bit grayscale and uniformly thresholded to distinguish particles from the background. Identical threshold settings were applied across all samples within each experiment to ensure consistency. Particle analysis was performed using the following parameters: size (25 pixels^2 to infinity; equivalent to ≥1 μm^2). The total number of particles per cell (or per image field) was recorded and subjected to statistical analysis.

Colocalization measurements were performed as previously described[14]. The percentage of overlapped area in the reference channel was used as the readout for each oocyte. For fluorescence intensity analysis, the mean cytoplasmic intensity of UBE2V1, γH2AX, ROS, OPP, EU, and LC3 was quantified from the equatorial section of each oocyte or embryo.

Statistics and reproducibility

Unless otherwise specified, all experiments were conducted with three biological replicates, with consistent results, as detailed in the figure legends.

Statistical analysis was performed using GraphPad Prism 9 (Student's *t*-test unless otherwise noted; data are presented as mean ± SD; $P < 0.05$ was considered significant). Sample sizes (n) and replicate definitions are specified in the figure legends. The raw data are available in the Supplementary Data.

Reporting summary

Further information on research design is available in the Nature Portfolio Reporting Summary linked to this article.

Data availability

The authors confirm that all data supporting this study are available: the supplementary source data are included in the Supplementary Information and Supplementary Data files, with additional data available from the corresponding authors upon reasonable request.

Received: 9 December 2024; Accepted: 13 May 2025;
Published online: 21 May 2025

References

1. Li, H. et al. The trend in delayed childbearing and its potential consequences on pregnancy outcomes: a single center 9-years retrospective cohort study in Hubei, China. *BMC Pregnancy Childbirth* **22**, 514–523 (2022).
2. Sauer, M. V. Reproduction at an advanced maternal age and maternal health. *Fertil. Steril.* **103**, 1136–1143 (2015).
3. Leridon, H. Can assisted reproduction technology compensate for the natural decline in fertility with age? A model assessment. *Hum. Reprod.* **19**, 1548–1553 (2004).
4. Bebbere, D., Coticchio, G., Borini, A. & Ledda, S. Oocyte aging: looking beyond chromosome segregation errors. *J. Assist. Reprod. Genet.* **39**, 793–800 (2022).
5. Webster, A. & Schuh, M. Mechanisms of aneuploidy in human eggs. *Trends Cell Biol.* **27**, 55–68 (2017).
6. Chiang, T., Duncan, F. E., Schindler, K., Schultz, R. M. & Lampson, M. A. Evidence that weakened centromere cohesion is a leading cause of age-related aneuploidy in oocytes. *Curr. Biol.* **20**, 1522–1528 (2010).
7. Lister, L. M. et al. Age-related meiotic segregation errors in mammalian oocytes are preceded by depletion of cohesin and Sgo2. *Curr. Biol.* **20**, 1511–1521 (2010).
8. Lane, S. I. & Jones, K. T. Non-canonical function of spindle assembly checkpoint proteins after APC activation reduces aneuploidy in mouse oocytes. *Nat. Commun.* **5**, 3444–3452 (2014).
9. Nabti, I., Grimes, R., Sarna, H., Marangos, P. & Carroll, J. Maternal age-dependent APC/C-mediated decrease in securin causes premature sister chromatid separation in meiosis II. *Nat. Commun.* **8**, 15346–15354 (2017).
10. Nakagawa, S. & FitzHarris, G. Intrinsically defective microtubule dynamics contribute to age-related chromosome segregation errors in mouse oocyte meiosis-I. *Curr. Biol.* **27**, 1040–1047 (2017).
11. Li, L., Zheng, P. & Dean, J. Maternal control of early mouse development. *Development* **137**, 859–870 (2010).
12. Xu, N. et al. Ube2v1 positively regulates protein aggregation by modulating ubiquitin proteasome system performance partially through K63 ubiquitination. *Circ. Res.* **126**, 907–922 (2020).
13. Koga, H., Kaushik, S. & Cuervo, A. M. Protein homeostasis and aging: the importance of exquisite quality control. *Ageing Res. Rev.* **10**, 205–215 (2011).
14. Zaffagnini, G. et al. Mouse oocytes sequester aggregated proteins in degradative super-organelles. *Cell* **187**, 1109–1126.e1121 (2024).
15. Stewart, M. D., Ritterhoff, T., Klevit, R. E. & Brzovic, P. S. E2 enzymes: more than just middle men. *Cell Res.* **26**, 423–440 (2016).
16. Yuan, L. et al. Single-cell transcriptome analysis of human oocyte ageing. *J. Cell. Mol. Med.* **25**, 6289–6303 (2021).
17. De Franceschi, N. et al. Selective integrin endocytosis is driven by interactions between the integrin α-chain and AP2. *Nat. Struct. Mol. Biol.* **23**, 172–179 (2016).
18. Zhang, G. et al. UBE2D3 functions in mouse oocyte meiotic maturation. *FASEB J.* **39**, e70375 (2025).
19. Jao, C. Y. & Salic, A. Exploring RNA transcription and turnover in vivo by using click chemistry. *Proc. Natl. Acad. Sci. USA* **105**, 15779–15784 (2008).
20. Hashimoto, M., Rockenstein, E., Crews, L. & Masliah, E. Role of protein aggregation in mitochondrial dysfunction and neurodegeneration in Alzheimer's and Parkinson's diseases. *Neuromolecular Med.* **4**, 21–36 (2003).
21. Wu, X. et al. NMNAT2-mediated NAD(+) generation is essential for quality control of aged oocytes. *Aging Cell* **18**, e12955 (2019).
22. Wen, J. H. et al. Cellular protein aggregates: formation, biological effects, and ways of elimination. *Int. J. Mol. Sci.* **24**, 1–14 (2023).
23. Susor, A. et al. Temporal and spatial regulation of translation in the mammalian oocyte via the mTOR-eIF4F pathway. *Nat. Commun.* **6**, 6078–6089 (2015).
24. Forester, C. M. et al. Revealing nascent proteomics in signaling pathways and cell differentiation. *Proc. Natl. Acad. Sci. USA* **115**, 2353–2358 (2018).
25. Knowles, T. P., Vendruscolo, M. & Dobson, C. M. The amyloid state and its association with protein misfolding diseases. *Nat. Rev. Mol. cell Biol.* **15**, 384–396 (2014).
26. Ayyadevara, S. et al. Age- and hypertension-associated protein aggregates in mouse heart have similar proteomic profiles. *Hypertension* **67**, 1006–1013 (2016).
27. Askanas, V., Engel, W. K. & Nogalska, A. Inclusion body myositis: a degenerative muscle disease associated with intra-muscle fiber multi-protein aggregates, proteasome inhibition, endoplasmic reticulum stress and decreased lysosomal degradation. *Brain Pathol.* **19**, 493–506 (2009).
28. Kopacz, A. et al. Keap1 governs ageing-induced protein aggregation in endothelial cells. *Redox Biol.* **34**, 101572–101586 (2020).
29. Secomandi, L., Borghesan, M., Velarde, M. & Demaria, M. The role of cellular senescence in female reproductive aging and the potential for senotherapeutic interventions. *Hum. Reprod. Update* **28**, 172–189 (2022).
30. Satouh, Y. et al. Endosomal-lysosomal organellar assembly (ELYSA) structures coordinate lysosomal degradation systems through mammalian oocyte-to-embryo transition. *eLife* **13**, 1–25 (2025).
31. Wang, G. et al. K63-linked ubiquitination in kinase activation and cancer. *Front. Oncol.* **2**, 5–17 (2012).
32. Guo, J. et al. Selective translation of maternal mRNA by eIF4E1B controls oocyte to embryo transition. *Adv. Sci.* **10**, e2205500 (2023).
33. Zhang, C., Wang, M., Li, Y. & Zhang, Y. Profiling and functional characterization of maternal mRNA translation during mouse maternal-to-zygotic transition. *Sci. Adv.* **8**, eabj3967 (2022).
34. Han, L. et al. Embryonic defects induced by maternal obesity in mice derive from Stella insufficiency in oocytes. *Nat. Genet* **50**, 432–442 (2018).
35. Zhang, Z. et al. Alpha-ketoglutarate affects murine embryo development through metabolic and epigenetic modulations. *Reproduction* **158**, 123–133 (2019).
36. Zeng, J. et al. SIRT4 is essential for metabolic control and meiotic structure during mouse oocyte maturation. *Aging Cell* **17**, e12789 (2018).
37. Wang, D. et al. FKBP25 regulates meiotic apparatus during mouse oocyte maturation. *Front. Cell Dev. Biol.* **9**, 625805–625815 (2021).

Acknowledgements

This work was supported by National Natural Science Foundation of China (NO. 82301877 to L.L.; NO. 82271689 to L.H.), Science Foundation of Jiangsu Province (BK20230058 to L.H.; BK20240728 to X.H.; BK20240725

to J.C), The Major Project of Colleges and Universities in Jiangsu Province (22KJA310001 to L.H.), and Traditional Chinese Medicine Technology Development Project of Jiangsu Province (ZD202302) to X.W.G.

Author contributions

L.L. and Y.L. performed the experiments and collected the data; Y.L., X.H., and J.C. assisted with animal model construction. L.L., Y.L., and L.H. analyzed data; L.H. and X.G. conceptualized and supervised the project; L.H wrote manuscript.

Competing interests

The authors declare no competing interests.

Additional information

Supplementary information The online version contains supplementary material available at https://doi.org/10.1038/s42003-025-08214-5.

Correspondence and requests for materials should be addressed to Xiaowei Guan or Longsen Han.

Peer review information *Communications Biology* thanks Alberto M. Luciano and the other, anonymous, reviewers for their contribution to the peer review of this work. Primary Handling Editors: Rupinder Kaur and Kaliya Georgieva.